IEEJ Journal of Industry Applications
Vol.7 No.1 pp.56–63 DOI: 10.1541/ieejjia.7.56

Paper

Behavior Modeling of Permanent Magnet Synchronous Motors Using Flux Linkages for Coupling with Circuit Simulation

Hiroyuki Kaimori[*a)] Member, Kan Akatsu[*] Member

(Manuscript received Feb. 17, 2017, revised July 25, 2017)

Accurate PMSM drive simulation, which utilizes a behavior model developed using FEA results to consider nonlinear characteristics, has been requested to evaluate driving performance. This paper proposes an advanced motor behavior model that is based on the flux linkage model instead of the inductance model to simplify the derivation of equations and to reduce the amount of table data produced from FEA results. The proposed model includes magnetic saturation, cross-coupling, and spatial harmonics. Its performance is verified in circuit simulation by comparing direct FEA results with measurement results. The results obtained using the proposed model are in good agreement well with the FEA results and measurement results.

Keywords: behavior modeling, cross-coupling, spatial harmonics, coupled analysis, finite element analysis (FEA), permanent magnet synchronous motor (PMSM)

1. Introduction

Permanent magnet synchronous motors (PMSMs) are widely used for industrial applications nowadays. Especially Interior PMSMs (IPMSMs) deliver the great performance at the high-efficiency over wide speed and torque ranges. Therefore, various control motor models have been proposed to achieve the high-performance [(1)–(3)].

In the design of PMSM drive systems, circuit simulations using a motor model which has constant parameters are typically implemented. The PMSM model is developed from FEA results at the specific driving condition such as the rated speed operation. Recently, in order to accurately simulate the nonlinear characteristics of PMSMs, a coupled analysis by using a motor behavior model produced from the FEA results is applied to the circuit simulation [(4)–(6)]. A motor behavior model, which precisely behaves a real motor in a circuit simulation, is desirable because the model can take into account the nonlinear effects due to the magnetic saturation, cross-coupling, and spatial harmonics. This analysis technique has been improved to be alternative for experimental evaluations in the previous researches. The direct-coupled analysis between the FEA and a circuit simulation has the high accuracy in the analysis of PMSM drives is well known [(7)]. However, this method is quite time-consuming. On the contrary, the analysis using the motor behavior model simulates the PMSM drive system in a very short time because it is implemented by calculating some equations for the dynamic response.

The performance of the motor behavior model depends on the modeling-accuracy of machine parameters such as the inductance and flux linkage. In general, the dynamic response of PMSMs is analyzed by calculating the voltage equation expressed with the inductance and flux linkage due to the permanent magnets [(4)(6)]. However, these models assume constant parameters which neglect the spatial harmonics effect caused by the stator slots. In Ref. (5), the three-phase inductance model is proposed to include the spatial harmonics even though neglecting the cross-coupling effect. Moreover, these solutions require the complicated calculation procedure to separate the flux linkage due to the inductance and it due to the permanent magnets from the total stator flux linkage. In addition, a lot of parameters must be employed in the coupled analysis.

In this paper, an advanced motor behavior model based on the total stator flux linkage is proposed to apply to the coupled analysis. The proposed method can be simply implemented to consider the magnetic saturation, cross-coupling and spatial harmonics. Therefore, the proposed model is applicable to circuit simulations under the flux-weakening and over modulation conditions in which the effect of the slot harmonics is significant. The coupled-analyses using the advanced behavior model are performed to verify the performance by the circuit simulation of PMSM drives.

2. Constant Parameter Model of a PMSM

In previous researches, three approaches to develop motor behavior models have been proposed in the *d-q* rotational reference frame. In the first one, the modeling of PMSMs is based on the voltage equation expressed with the self-inductances. The other methods use the rigorous model which includes the parameters such as the self- and mutual inductances and flux linkages. The detail of the existing approaches in the *d-q* rotational reference frame is discussed in the following section.

2.1 Self-Inductance Model In general, the voltage equation of PMSMs in the *d-q* rotational reference frame is expressed with constant parameters as follows:

a) Correspondence to: Hiroyuki Kaimori. E-mail: kaimorih@ssil.co.jp
* Science Solutions International Laboratory, Inc.
2-21-7, Naka-cho, Meguro-ku, Tokyo 153-0065, Japan

$$\begin{bmatrix} v_d \\ v_q \end{bmatrix} = R_a \begin{bmatrix} i_d \\ i_q \end{bmatrix} + \begin{bmatrix} pL_d & -\omega_r L_q \\ \omega_r L_d & pL_q \end{bmatrix} \begin{bmatrix} i_d \\ i_q \end{bmatrix} + \begin{bmatrix} 0 \\ \omega_r \psi_m \end{bmatrix} \cdots\cdots (1)$$

where v_d, v_q, i_d, i_q, L_d, L_q are the d- and q-axis voltages, currents, self-inductances, respectively, and R_a is the armature winding resistance, ψ_m is the flux linkage due to the permanent magnets, ω_r is the angler rotational velocity, and $p = d/dt$. The inductances are defined as,

$$L_d = \frac{\psi_{0d} - \psi_m}{i_d}, \quad L_q = \frac{\psi_{0q}}{i_q} \cdots\cdots\cdots\cdots\cdots\cdots (2)$$

where ψ_{0d} and ψ_{0q} are the d- and q-axis flux linkages, respectively.

Considering the cross-coupling and magnetic saturation, the inductances can be written as,

$$L_d\left(i_d, i_q\right) = \frac{\psi_{0d}\left(i_d, i_q\right) - \psi_m}{i_d}, \quad L_q\left(i_d, i_q\right) = \frac{\psi_{0q}\left(i_d, i_q\right)}{i_q} \cdots\cdots\cdots\cdots\cdots\cdots (3)$$

where ψ_m is constant. Furthermore, to improve the accuracy of the torque calculation, ψ_m is defined considering the current dependency as follows [6]:

$$\psi_m\left(i_q\right) = \psi_{0d}\left(i_d = 0, i_q\right)$$
$$L_d\left(i_d, i_q\right) = \frac{\psi_{0d}\left(i_d, i_q\right) - \psi_m\left(i_q\right)}{i_d}, \; L_q\left(i_d, i_q\right) = \frac{\psi_{0q}\left(i_d, i_q\right)}{i_q}. \cdots\cdots\cdots\cdots\cdots\cdots (4)$$

Although $\psi_m(i_q)$ can consider the magnetic saturation, ψ_m is also affected by i_d. However, it is relatively difficult to separate these fluxes: the flux due to the magnets and it due to the stator current on the d-axis from the total stator flux linkage. Namely, the definition of L_d and ψ_m remains the difficulty for the current dependency.

In PMSMs, the mean torque T_e can be calculated from

$$T_e = P_n\left\{\psi_m i_q + \left(L_d - L_q\right) i_d i_q\right\} \cdots\cdots\cdots\cdots\cdots\cdots (5)$$

where P_n is the number of pole pairs.

2.2 Inductance Matrix Model Considering the cross-coupling to express the mutual inductances, the d- and q-axis flux linkages can be defined as

$$\begin{bmatrix} \psi_{0d}\left(i_d, i_q\right) \\ \psi_{0q}\left(i_d, i_q\right) \end{bmatrix} = \begin{bmatrix} L_{dd}\left(i_d, i_q\right) & L_{dq}\left(i_d, i_q\right) \\ L_{qd}\left(i_d, i_q\right) & L_{qq}\left(i_d, i_q\right) \end{bmatrix} \begin{bmatrix} i_d \\ i_q \end{bmatrix} + \begin{bmatrix} \psi_m \\ 0 \end{bmatrix} \cdots\cdots\cdots\cdots\cdots\cdots (6)$$

where $L_{dd}(= L_d)$, $L_{qq}(= L_q)$, and L_{dq}, L_{qd} are the d- and q-axis self- and mutual inductances, respectively. The cross-coupling effect is determined by the parameters L_{dq}, L_{qd}. Substituting (6) into (1) gives the following equation [4],

$$\begin{bmatrix} v_d \\ v_q \end{bmatrix} = R_a \begin{bmatrix} i_d \\ i_q \end{bmatrix} + \begin{bmatrix} L_{dd}\left(i_d, i_q\right) & L_{dq}\left(i_d, i_q\right) \\ L_{qd}\left(i_d, i_q\right) & L_{qq}\left(i_d, i_q\right) \end{bmatrix} \begin{bmatrix} \dfrac{di_d}{dt} \\ \dfrac{di_q}{dt} \end{bmatrix} + \omega_r \begin{bmatrix} -L_{qd}\left(i_d, i_q\right) & -L_{qq}\left(i_d, i_q\right) \\ L_{dd}\left(i_d, i_q\right) & L_{dq}\left(i_d, i_q\right) \end{bmatrix} \begin{bmatrix} i_d \\ i_q \end{bmatrix} + \begin{bmatrix} 0 \\ \omega_r \psi_m \end{bmatrix}. \cdots\cdots\cdots\cdots\cdots\cdots (7)$$

In (7), the L_{dd}, L_{qq}, L_{dq}, and L_{qd} are independent of time differential p. According to Ref. (4), these inductances can be defined by (8) where the ψ_m is constant,

$$\begin{cases} L_{dd} = \dfrac{\partial \psi_{0d}(i_d, i_q)}{\partial i_d} = \dfrac{\psi_{0d}(i_d + \Delta i_d, i_q) - \psi_{0d}(i_d, i_q)}{\Delta i_d} \\ L_{qq} = \dfrac{\partial \psi_{0q}(i_d, i_q)}{\partial i_q} = \dfrac{\psi_{0q}(i_d, i_q + \Delta i_q) - \psi_{0q}(i_d, i_q)}{\Delta i_q} \\ L_{dq} = \dfrac{\partial \psi_{0d}(i_d, i_q)}{\partial i_q} = \dfrac{\psi_{0d}(i_d, i_q + \Delta i_q) - \psi_{0d}(i_d, i_q)}{\Delta i_q} \\ L_{qd} = \dfrac{\partial \psi_{0q}(i_d, i_q)}{\partial i_d} = \dfrac{\psi_{0q}(i_d + \Delta i_d, i_q) - \psi_{0q}(i_d, i_q)}{\Delta i_d} \end{cases} \cdots\cdots\cdots\cdots\cdots\cdots (8)$$

where Δi_d and Δi_q are incremental d- and q-axis currents, respectively. Here, it should be noted that the value obtained from (8) is technically called as the differential (incremental) inductances. Under the strong magnetic saturation condition, the calculated differential inductance is inaccurate against the inductances such as calculated by (4) because of the linear assumption. Also, the calculation needs at least three case analysis results for each driving condition.

By using expression (8), T_e can be rewritten as follows:

$$T_e = P_n\left\{\psi_m i_q + \left(L_{dd} - L_{qq}\right) i_d i_q - L_{qd} i_d^2 + L_{dq} i_q^2\right\} \cdots\cdots (9)$$

where $L_{qd} i_d^2$ and $L_{dq} i_q^2$ express the terms of the cross-coupling torques.

2.3 Flux Linkage Model The flux linkage model has been investigated for synchronous reluctance motors and verified its accuracy [8][9]. This model enables to consider the magnetic saturation and cross-coupling. The model can be also used for PMSM. The equation can be written as follows:

$$\begin{bmatrix} v_d \\ v_q \end{bmatrix} = R_a \begin{bmatrix} i_d \\ i_q \end{bmatrix} + \begin{bmatrix} p & -\omega_r \\ \omega_r & p \end{bmatrix} \begin{bmatrix} \psi_{0d} \\ \psi_{0q} \end{bmatrix} \cdots\cdots\cdots\cdots\cdots\cdots (10)$$

In (10), the voltage equation is expressed with the flux linkage due to the armature current ($L_d i_d$, $L_q i_q$) and the permanent magnets.

T_e is calculated from

$$T_e = P_n\left(\psi_{0d} i_q - \psi_{0q} i_d\right) \cdots\cdots\cdots\cdots\cdots\cdots (11)$$

2.4 Relation with Those Models for FEA The point of the accuracy of the motor behavior models is how to treat the nonlinear parameters to keep the same accuracy as the FEA results. Considering magnetic saturation and cross-coupling, the inductances or flux linkages are treated as the nonlinear parameters. The FEA analysis consider the nonlinear magnetic materials as the function of magnetic density B and magnetic intensity H, $H = H(B)$. For coupling with electrical circuit in FEA, the inductances or flux linkage of coils should be nonlinear as $\psi = L(i) = \psi(i)$ in the same way as the nonlinear magnetic materials. By the definition of the inductance, the stator flux linkage requires to separate the inductance term and permanent magnets term. However, the flux linkage of the stator coil in FEA analysis is no doubt to be included both nonlinear effect of magnetic saturation and cross-coupling. This is very difficult to divide them even using FEA. The performance of the FEA results is not our present concern because its accuracy was already proved in previous research [7]. Therefore, we limit the discussion to the verification of the motor behavior model.

3. Advanced Modeling Considering Spatial Harmonics

As mentioned above, constant parameters are applied to these three models of PMSM. However, to evaluate PMSM drive systems an accurate motor model which can take into account the slot effect (spatial harmonics) is required in the circuit simulation. By using the rigorous model, the precise analysis considering not only the time harmonics but also the spatial harmonics is possible to adapt the circuit simulation.

To determine the parameters considering the spatial harmonics, the FEA results including the rotation angle θ is applied to the PMSM model. Consequently, the self-inductances model can be expressed as the function of θ. Therefore, (1) can be rewritten as follows:

$$\begin{bmatrix} v_d \\ v_q \end{bmatrix} = R_a \begin{bmatrix} i_d \\ i_q \end{bmatrix} + \begin{bmatrix} L_d\left(i_d, i_q, \theta\right) \\ L_q\left(i_d, i_q, \theta\right) \end{bmatrix} \begin{bmatrix} \dfrac{di_d}{dt} \\ \dfrac{di_q}{dt} \end{bmatrix} + \omega_r \begin{bmatrix} \dfrac{dL_d\left(i_d, i_q, \theta\right)}{d\theta} & -L_q\left(i_d, i_q, \theta\right) \\ L_d\left(i_d, i_q, \theta\right) & \dfrac{dL_q\left(i_d, i_q, \theta\right)}{d\theta} \end{bmatrix} \begin{bmatrix} i_d \\ i_q \end{bmatrix} + \begin{bmatrix} 0 \\ \omega_r \psi_m(\theta) \end{bmatrix}, \quad \cdots\cdots\cdots\cdots (12)$$

$dL_d(i_d, i_q, \theta)/d\theta$, $dL_q(i_d, i_q, \theta)/d\theta$ express the terms of the considered spatial harmonics in (12). The three parameters, such as $L_d(i_d, i_q, \theta)$, $L_q(i_d, i_q, \theta)$ and $\psi_m(\theta)$ (or $\psi_m(i_d = 0, i_q, \theta)$) need each i_d, i_q, θ with the table data for coupled analysis with the circuit simulation.

Likewise, (7) can be rewritten as follows:

$$\begin{bmatrix} v_d \\ v_q \end{bmatrix} = R_a \begin{bmatrix} i_d \\ i_q \end{bmatrix} + \begin{bmatrix} L_{dd}\left(i_d, i_q, \theta\right) & L_{dq}\left(i_d, i_q, \theta\right) \\ L_{qd}\left(i_d, i_q, \theta\right) & L_{qq}\left(i_d, i_q, \theta\right) \end{bmatrix} \begin{bmatrix} \dfrac{di_d}{dt} \\ \dfrac{di_q}{dt} \end{bmatrix} + \omega_r \begin{bmatrix} \dfrac{dL_{dd}\left(i_d, i_q, \theta\right)}{d\theta} & \dfrac{dL_{dq}\left(i_d, i_q, \theta\right)}{d\theta} \\ \dfrac{dL_{qd}\left(i_d, i_q, \theta\right)}{d\theta} & \dfrac{dL_{qq}\left(i_d, i_q, \theta\right)}{d\theta} \end{bmatrix} \begin{bmatrix} i_d \\ i_q \end{bmatrix} + \omega_r \begin{bmatrix} -L_{qd}\left(i_d, i_q, \theta\right) & -L_{qq}\left(i_d, i_q, \theta\right) \\ L_{dd}\left(i_d, i_q, \theta\right) & L_{dq}\left(i_d, i_q, \theta\right) \end{bmatrix} \begin{bmatrix} i_d \\ i_q \end{bmatrix} + \begin{bmatrix} 0 \\ \omega_r \psi_m(\theta) \end{bmatrix}, \quad \cdots\cdots\cdots\cdots (13)$$

$dL_{dd}(i_d, i_q, \theta)/d\theta$, $dL_{dq}(i_d, i_q, \theta)/d\theta$, $dL_{qd}(i_d, i_q, \theta)/d\theta$, $dL_{qq}(i_d, i_q, \theta)/d\theta$ express the terms of the considered spatial harmonics in (13). Likewise, the five parameters, such as the $L_{dd}(i_d, i_q, \theta)$, $L_{dq}(i_d, i_q, \theta)$, $L_{qd}(i_d, i_q, \theta)$, $L_{qq}(i_d, i_q, \theta)$ and $\psi_m(\theta)$ need each i_d, i_q, θ with the table data.

On the contrary, in the flux linkage model, the spatial harmonics are simply expressed in (10) as follows:

$$\begin{bmatrix} v_d \\ v_q \end{bmatrix} = R_a \begin{bmatrix} i_d \\ i_q \end{bmatrix} + \begin{bmatrix} \dfrac{d\psi_{0d}(i_d, i_q, \theta)}{dt} \\ \dfrac{d\psi_{0q}(i_d, i_q, \theta)}{dt} \end{bmatrix} + \omega_r \begin{bmatrix} -\psi_{0q}(i_d, i_q, \theta) \\ \psi_{0d}(i_d, i_q, \theta) \end{bmatrix}. \quad \cdots\cdots\cdots\cdots (14)$$

In this case, the only two parameters, such as $\psi_{0d}(i_d, i_q, \theta)$ and $\psi_{0q}(i_d, i_q, \theta)$ need at each i_d, i_q, θ with the table data.

In this paper, we propose to apply the Newton-Raphson method to the nonlinear calculation of the flux linkage model because the flux linkage model is the simplest in the others.

Considering the current-dependent, (14) is rewritten for the Newton-Raphson method as follows:

$$\boldsymbol{R}\left(\boldsymbol{i}^{(k)}\right) = \frac{1}{R_a}\begin{bmatrix} v_d \\ v_q \end{bmatrix} - \begin{bmatrix} i_d^{(k)} \\ i_q^{(k)} \end{bmatrix} - \frac{1}{R_a}\begin{bmatrix} p & -\omega_r \\ \omega_r & p \end{bmatrix} \begin{bmatrix} \psi_{0d}(i_d^{(k)}, i_q^{(k)}) \\ \psi_{0q}(i_d^{(k)}, i_q^{(k)}) \end{bmatrix} \quad \cdots\cdots\cdots\cdots (15)$$

The residual $\boldsymbol{R}(\boldsymbol{i}^{(k)})$ at the k-th nonlinear iteration by Taylor expansion of (15) is given as,

$$\begin{aligned} \boldsymbol{R}\left(\boldsymbol{i}^{(k+1)}\right) &= \boldsymbol{R}\left(\boldsymbol{i}^{(k)} + \delta\boldsymbol{i}^{(k)}\right) \\ &= \boldsymbol{R}\left(\boldsymbol{i}^{(k)}\right) + \frac{\partial \boldsymbol{R}^{(k)}}{\partial \boldsymbol{i}^{(k)}}\partial\boldsymbol{i}^{(k)} + \boldsymbol{O}\left(\partial\boldsymbol{i}^{(k)^2}\right). \cdots\cdots (16) \end{aligned}$$

Omitting the 3rd term $\boldsymbol{O}(\delta\boldsymbol{i}^{(k)2})$, (16) gives linear equations with respect to $\delta\boldsymbol{i}^{(k)}$ as,

$$\begin{aligned} \boldsymbol{r}\left(\delta\boldsymbol{i}^{(k)}\right) &= \boldsymbol{R}\left(\boldsymbol{i}^{(k)}\right) + \frac{\partial \boldsymbol{R}\left(\boldsymbol{i}^{(k)}\right)}{\partial \boldsymbol{i}^{(k)}} \\ &= \boldsymbol{R}\left(\boldsymbol{i}^{(k)}\right) - \frac{1}{R_a}\begin{bmatrix} p\dfrac{d\psi_{0d}(i_d^{(k)}, i_q^{(k)})}{di_d^{(k)}} & -\omega_r\dfrac{d\psi_{0q}(i_d^{(k)}, i_q^{(k)})}{di_q^{(k)}} \\ \omega_r\dfrac{d\psi_{0d}(i_d^{(k)}, i_q^{(k)})}{di_d^{(k)}} & p\dfrac{d\psi_{0q}(i_d^{(k)}, i_q^{(k)})}{di_q^{(k)}} \end{bmatrix} \begin{bmatrix} \delta i_d^{(k)} \\ \delta i_q^{(k)} \end{bmatrix} = 0 \\ & \cdots\cdots\cdots\cdots\cdots\cdots (17) \end{aligned}$$

where $d\psi_{0d}(i_d^{(k)}, i_q^{(k)})/di_d^{(k)}$ and $d\psi_{0q}(i_d^{(k)}, i_q^{(k)})/di_q^{(k)}$ are nonlinear terms. The process to solve the nonlinear calculation is as follows:

1) The initial value of $d\psi_{0d}(i_d^{(0)}, i_q^{(0)})/di_d^{(0)}$ and $d\psi_{0q}(i_d^{(0)}, i_q^{(0)})/di_q^{(0)}$ are determined.
2) $\delta i_d^{(0)}$ and $i_q^{(0)}$ are set to zero.
3) i_d and i_q is updated by $i_d^{(k)} = i_d^{(k-1)} + \delta i_d^{(k)}$ and $i_q^{(k)} = i_q^{(k-1)} + \delta i_q^{(k)}$ using $\delta i_d^{(k)}$ and $\delta i_q^{(k)}$ calculated by (17).
4) $\psi_{0d}^{(k)}$ and $\psi_{0q}^{(k)}$ are calculated using the table data $i_d^{(k)}$ and $i_q^{(k)}$.
5) The process from 3) to 5) is repeated.
6) It is judged to be converged if $\boldsymbol{r}(\delta\boldsymbol{i}^{(k)})$ is less than a specified small value which means i_d and i_q obtain sufficiently accurate.

The parameters are typically calculated in advance by FEA for the coupling analysis [5]. $\psi_{0d}(i_d, i_q)$ and $\psi_{0q}(i_d, i_q)$ can be stored in the look-up table. One can be stored in the d- and q-axis frame data structure as shown in Fig. 1(a). As shown in the figure, the d- and q-axis data structure is not ordered in i_d and i_q, that is needed 2-D index data and must use special searching methods such as hash table. The other way, such data structure is converted to the amplitude and phase frame data structure. As shown in Fig. 1(b) in the amplitude and phase frame data structure, it is clear to treat easily by searching method. Moreover, the computational cost can reduce by using the amplitude and phase frame data structure because of its generality.

The d- and q-axis currents can be expressed with the current vector length I_a and vector phase β, as shown in Fig. 1(b), these relationships are defined as follow

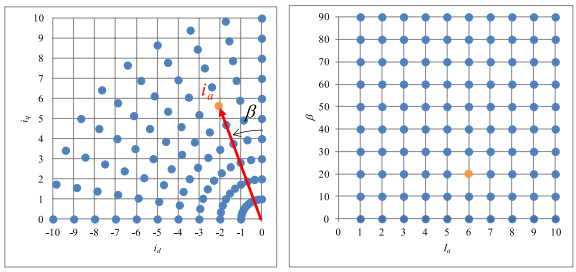

(a) i_d-i_q table. (b) I_a-β table.

Fig. 1. Table data structures

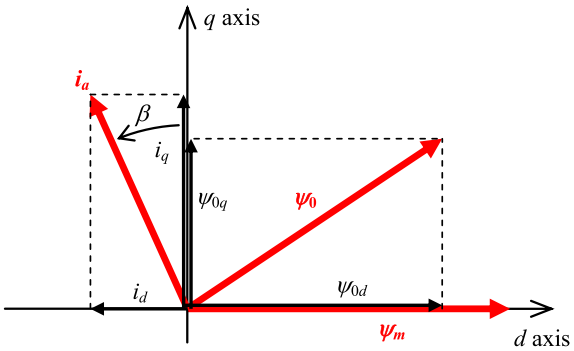

Fig. 2. Current, voltage, and flux linkage vectors on d-q reference frame

$$I_a = \sqrt{i_d^2 + i_q^2}, \quad \beta = -\arctan\left(\frac{i_d}{i_q}\right). \cdots\cdots\cdots\cdots (18)$$

Figure 2 shows the relationship of the armature current vector on the d-q reference frame.

By using I_a and β in (18) expression, the nonlinear terms of (17) can be transformed as follows:

$$\frac{d\psi_{0d}\left(i_d^{(k)}, i_q^{(k)}\right)}{di_d^{(k)}} = -\frac{d\psi_{0d}\left(I_a^{(k)}, \beta^{(k)}\right)}{dI_a^{(k)}}\sin\beta^{(k)} - \frac{\cos\beta^{(k)}}{I_a^{(k)}}\frac{d\psi_{0d}\left(I_a^{(k)}, \beta^{(k)}\right)}{d\beta^{(k)}}, \cdots\cdots\cdots\cdots (19)$$

$$\frac{d\psi_{0q}\left(i_d^{(k)}, i_q^{(k)}\right)}{di_q^{(k)}} = \frac{d\psi_{0q}\left(I_a^{(k)}, \beta^{(k)}\right)}{dI_a^{(k)}}\cos\beta^{(k)} - \frac{\sin\beta^{(k)}}{I_a^{(k)}}\frac{d\psi_{0q}\left(I_a^{(k)}, \beta^{(k)}\right)}{d\beta^{(k)}}, \cdots\cdots\cdots\cdots (20)$$

where $d\psi_{0d}(I_a^{(k)}, \beta^{(k)})/dI_a^{(k)}$ and $d\psi_{0q}(I_a^{(k)}, \beta^{(k)})/d\beta^{(k)}$ are rewritten as the nonlinear terms.

Adding that, the torque ripple due to the spatial harmonics can be taken into account by using the FEA results in the above modeling of PMSMs.

In previous researches, three approaches to develop motor behavior models have been proposed in the d-q rotational reference frame. In the first one, the modeling of PMSMs is based on the voltage equation expressed with the self-inductances. The other methods use the rigorous model which includes the parameters such as the self- and mutual inductances and flux linkages. The detail of the existing approaches in the d-q rotational reference frame is discussed in the following section.

4. Behavior Model Verifications

As an IPMSM benchmark motor, "D1 model" was proposed by a committee in the IEE of Japan to compare the FEA and the measurement results [10]. In this paper, this benchmark motor is used as the tested machine. The mesh of the benchmark motor and the specification is shown in Fig. 3 and Table 1, respectively. The motor is 4-poles and it has a concentrated-winding. As shown in Fig. 3, the half mesh model is applied to the 2D FEA. The eddy current losses of the permanent magnet and the iron core losses are neglected in the analysis.

Figure 4 shows the mean torque-current characteristic at β = 0 deg. condition. In this result, torques calculated by (5) and (11) are compared with the one obtained by the FEA. The torque-current characteristic obtained by (5) is perfectly linear because ψ_m is assumed as the constant that it is independent from i_d or i_q. On the other hand, the result obtained by (11) shows the nonlinear characteristic of current increasing because the model is based on the flux linkage which can take into account the dependent from i_d or i_q for magnetic saturation and the cross-coupling. Therefore, the result by (11) agrees fairly well with the one by the FEA.

Figure 5 shows the current phase-inductance characteristic calculated by (3). As shown in Fig. 5, the inductances have current-dependence. Figure 6 shows the current phase-flux linkage characteristic to compare with Fig. 5. As well

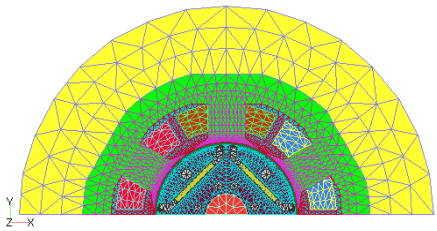

Fig. 3. Two-dimensional mesh of (tested PMSM) D1 model

Table 1. Specification of (tested PMSM) D1 model

Number of poles	4
Number of stator slots	6
Maximum current [Arms]	7.5
Armature winding Resistance [Ω/phase]	0.38
Magnetization of magnet [T]	1.225
Grade of electrical steel sheet	35A300

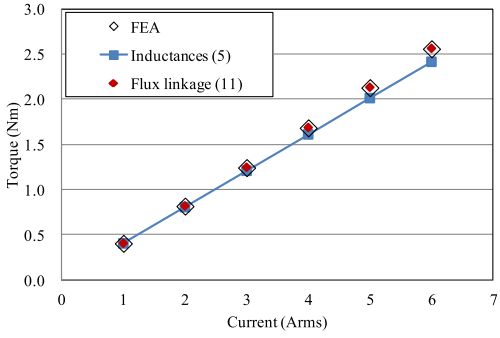

Fig. 4. Mean torque and current characteristic, $\beta = 0$

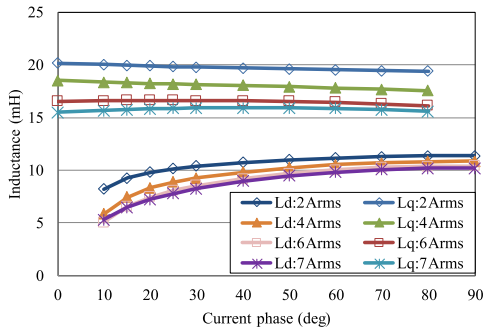

Fig. 5. Current phase and inductance characteristic calculated by (3)

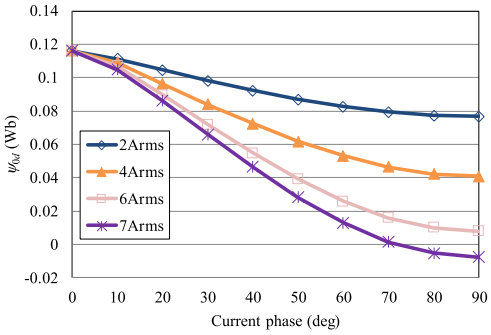

(a) ψ_{0d}

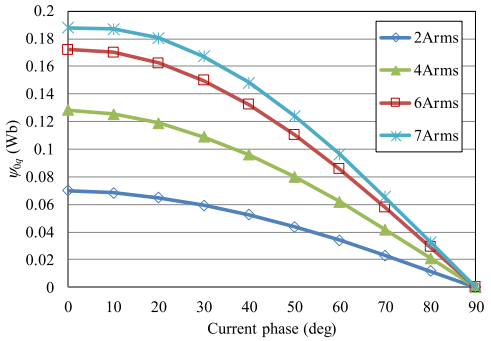

(b) ψ_{0q}

Fig. 6. Current phase and flux linkage characteristic

known, the L_d at $\beta = 0$ deg. and L_q at $\beta = 90$ deg. cannot be calculated because of $i_d = 0$ A at $\beta = 0$ deg. and $i_q = 0$ A at $\beta = 90$ deg. It seems to be one of the problems of the inductance models. On the contrary, the flux linkage as shown in Fig. 6 expresses naturally in all β. This is the better point of the flux linkage model because of no exception treatment in the coupling analysis. In addition, Fig. 7 shows the flux linkage distributions with the rotor position. As shown in Fig. 7, the inductances and flux linkages have spatially-dependence with currents and rotor positions. The flux linkage distribution includes the 6th harmonic component in the electric angle.

4.1 Rotor Position Dependence of Voltages Predicted by Alternative Models Figures 8, 9 shows the d- and q-axis voltage waveforms calculated by the FEA and behavior models. In this verification, the armature current is controlled at constant value on the d-q reference frame. The motor speed is 1500 min^{-1}. The operation points are $I_e = 4.4$ Arms, $\beta = 20$ deg. and $I_e = 7.5$ Arms, $\beta = 60$ deg. The FEA results are obtained by calculating in static analysis assuming a steady-state operation in the rated conditions. The inductances and

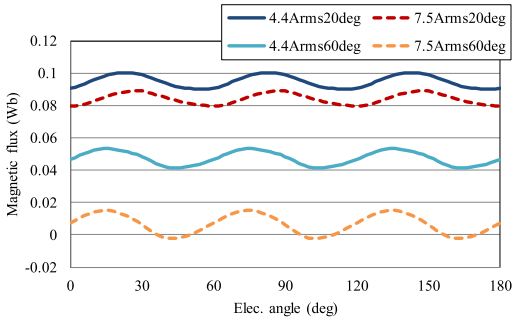

(a) ψ_{0d},

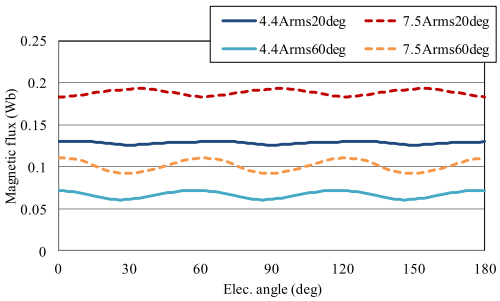

(b) ψ_{0q}

Fig. 7. Flux linkages with rotor position

the flux linkages are determined by these FEA results. In the calculation of (13), Δi_d and Δi_q are assumed 5% of the rated current.

As expected, v_q waveforms obtained by the self-inductance model of (12) and (12) with $\psi_m(i_q, \theta)$ of (4), and the flux linkage model of (14) are identical and agree excellent with the one by the FEA results. v_d waveforms obtained by the flux linkage model is also identical and agree excellent with the one by the FEA results. However, the results derived by both self-inductance models have different waveforms from the FEA results even though the mean values agree well with the one by the FEA results. On the contrary, both voltages by calculating the inductance matrix model of (13) are significantly different from the FEA results. This is because the linear assumption is applied to the calculation of (8). Thereby the difference is increased when I_e and β are increased. The difference of the inductance matrix model in Fig. 9 are extremely huge values, i.e. mean values are about -1500 V of V_d and 4600 V of V_q. As a result, the flux linkage model proves that it can obtain as same performance as the FEA.

4.2 Torque and Current Waveforms in Coupled Simulations by Proposed Model and Direct FEA The advanced motor behavior model used the flux linkage model to take into account the influence of cross-coupling, magnetic saturation, and spatial harmonics is developed in Simulink. As an example, a validation compared with the direct FEA coupling analysis under load conditions in the current control system for PMSM drive by Simulink is performed. A 200 V DC bus voltage is given. The advanced motor behavior model based on state equations (14), (16)–(19) are implemented in the subsystem. The current, current phase, rotor angle dependence of ψ_{0d}, ψ_{0q}, and torques are stored in data arrays and these are used in the calculation of the Newton-Raphson procedure. The momentum equation is used in the calculation of the rotor angle in this circuit simulation for its flexibility and

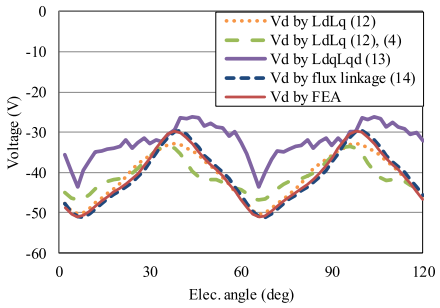

(a) V_d

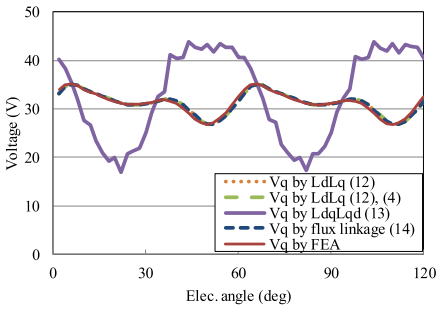

(b) V_q

Fig. 8. Variation of voltage with rotor position at I_e = 4.4 Arms, β = 20

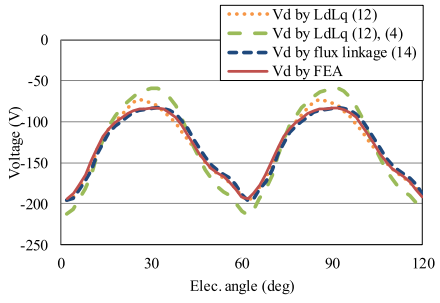

(a) V_d

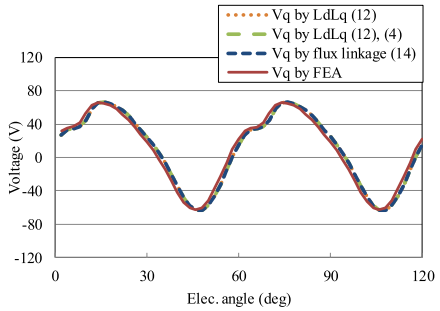

(b) V_q

Fig. 9. Variation of voltage with rotor position at I_e = 7.5 Arms, β = 60. (V_d, V_q by LdqLqd are out of range)

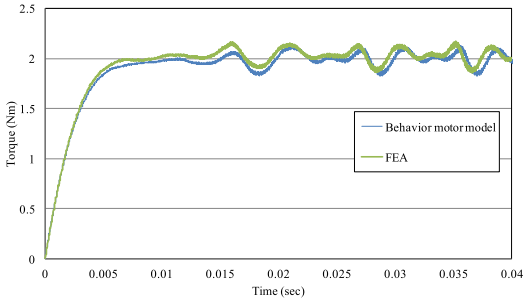

(a) Torque

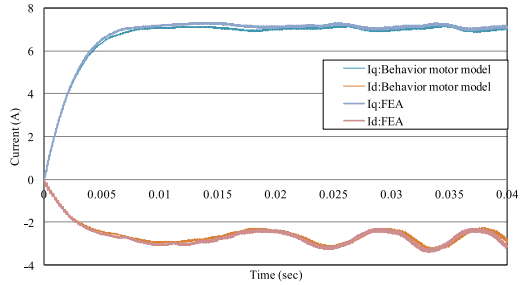

(b) i_d, i_q

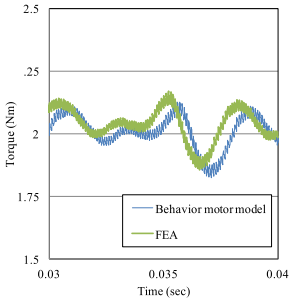

(c) Torque (enlargement)

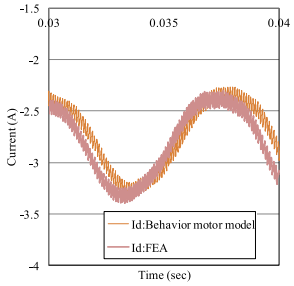

(d) i_d (enlargement)

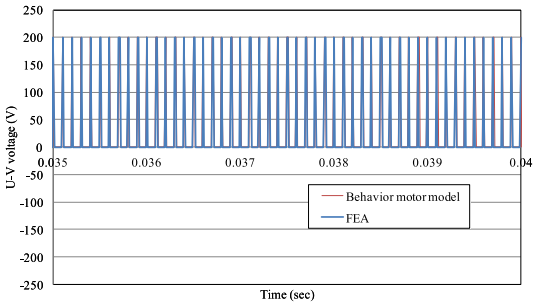

(e) U-V voltage (enlargement)

Fig. 10. Dynamic variations of coupled simulation under the rated operation point

expandability.

The dynamic performance comparison between the advanced motor behavior model and the direct FEA results under the rated operation is shown in Fig. 10. In the condition, I_e = 4.4 Arms, β = 20 deg. Initial speed is 0 min^{-1} then the acceleration of the electric machine is simulated by calculating the momentum equation block. The dynamic variation in the condition I_e = 7.5 Arms, β = 60 deg., 6000 min^{-1} as one of the examples of the flux-weakening and over modulation conditions nearly 95% ψ_{0d} weakening from β = 0 deg. is shown in Fig. 11. The torque, i_d, i_q waveforms obtained by the advanced behavior model agree excellent with the direct FEA results. This advanced motor behavior model can achieve the same performance in the viewpoint of the spatial harmonics and time domain representation with the direct FEA result as shown in enlarge views. The average torque, i_d, i_q have less than 2% error in both conditions. In addition, the torque ripple, peak-to-peak of i_d, i_q have less than 4% error in both conditions. As a result, the advanced motor behavior model proves that it can obtain as same performance as the direct FEA coupling analysis.

Table 2 shows the calculation times of the motor behavior model and direct FEA coupling analysis. As expected, the direct FEA coupling analysis is quite time-consuming. On the

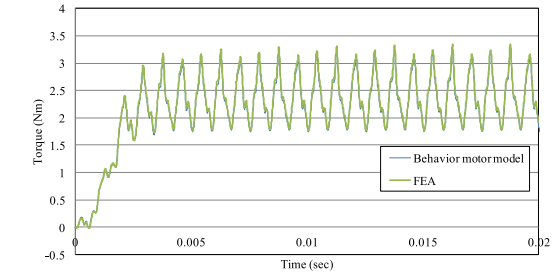

(a) Torque

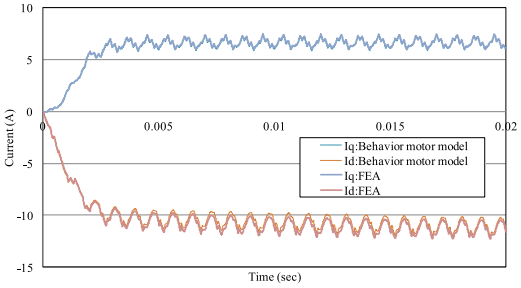

(b) i_d, i_q

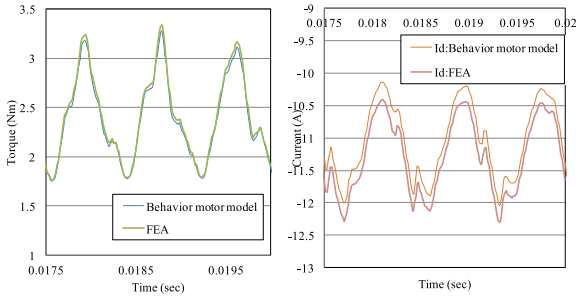

(c) Torque (enlargement) (d) i_d (enlargement)

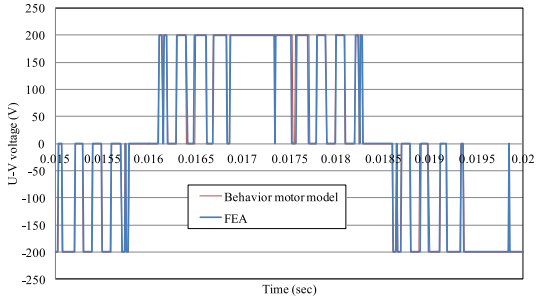

(e) U-V voltage (enlargement)

Fig. 11. Dynamic variations of coupled simulation under the flux-weakening and over modulation operation point

Table 2. Calculation times

Operation point	Rated	Over modulation
Simulation time	0.04s	0.02s
Motor behavior model	1.3s	0.9s
Direct FEA	6h56m	2h54m

contrary, the behavior model is much faster simulation times.

4.3 Current Waveforms by Proposed Model and Measurement The dynamic performance comparison with the advanced motor behavior model and the measurement under the steady-state condition as I_e = 4.4 Arms, β = 0 deg., 1500 min^{-1} is shown in Fig. 12. As shown in Fig. 12, the phase current has a closely fundamental waveform. The phase current waveform agrees fairly well with

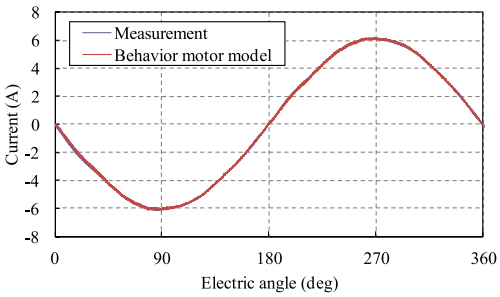

(a) Phase current

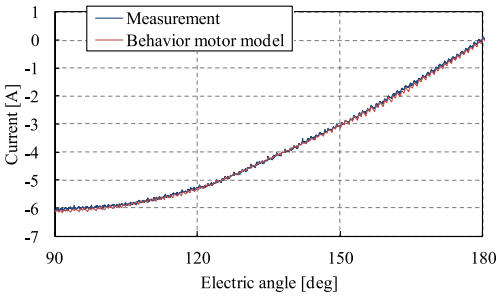

(b) Phase current (enlargement)

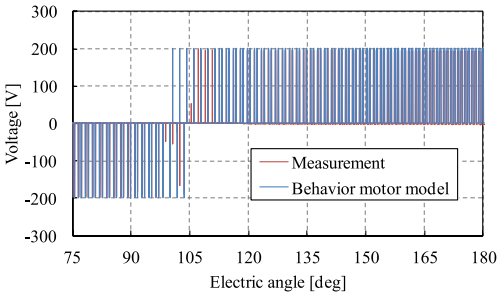

(c) Phase voltage (enlargement)

Fig. 12. Variations of simulation and measurement under the steady-state rated operation

the measurement even though the slight difference of the U-V voltage waveform is observed due to ignore the inverter dead time delay in the simulation. The fundamental phase current error is only less than 0.2% and the voltage error is only less than 2.0%. Figure 13 shows the dynamic performance comparison under the flux-weakening condition as I_e = 4.4 Arms, β = 68 deg, 3000 min^{-1} nearly 60% ψ_{0d} weakening from β = 0 deg., where the DC bus voltage is 140 V because of the limitation of the measurement system. Likewise, the phase current waveform agrees well with the measurement even though the phase current waveform has slightly distortion. The fundamental phase current has only less than 2.3% error. The biggest phase current harmonic; 5$^{\mathrm{th}}$ component is verified that they are 0.13 A and 0.15 A of the advanced motor behavior model and the measurement respectively. In this verification, the advanced motor behavior model can also achieve the same performance with the measurement result.

5. Conclusion

An advanced motor behavior model based on the flux linkage model is proposed to consider the cross-coupling, magnetic saturation, and spatial harmonics in the circuit simulation. The flux linkage model is proved the higher accuracy than the self-inductance model or the inductance matrix model. The dependent variables ψ_{0d}, ψ_{0q} are transformed

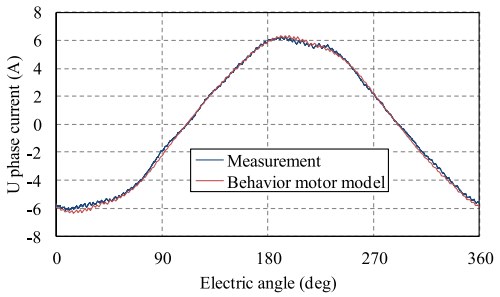

(a) Phase current

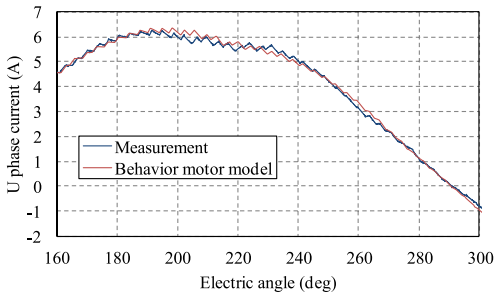

(b) Phase current (enlargement)

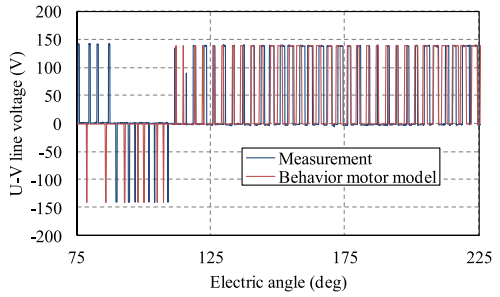

(c) Phase voltage (enlargement)

Fig. 13. Variations of simulation and measurement under the flux-weakening rated operation

from i_d, i_q to I_a, β applying the Newton-Raphson method for the amplitude and phase frame data structure. The accuracy and effectiveness of the proposed method are verified by comparing the torque, current, and voltage of the direct FEA and the measurement. Moreover, the circuit simulation time can be much faster than the direct FEA to obtain the same performance.

References

(1) S. Morimoto, Y. Takeda, T. Hirasa, and K. Taniguchi: “Expansion of Operating Limits for Permanent Magnet Motor by Current Vector Control Considering Inverter Capacity”, *IEEE Trans. Ind. Applicat.*, Vol.26, No.5, pp.866–871 (1990)

(2) H.W. de Kock, A.J. Rix, and M.J. Kamper: “Optimal Torque Control of Synchronous Machines Based on Finite-Element Analysis”, *IEEE Trans. Ind. Electron.*, Vol.57, No.1, pp.413–419 (2010)

(3) H. Nagura, Y. Iwaji, J. Nakatsugawa, and N. Iwasaki: “New Vector Controller for PM Motors which Modeled the Cross-Coupling Magnetic Flux Saturation”, 2010 International Power Electronics Conference (IPEC), pp.1064–1070 (2010)

(4) B. Stumberger, G. Stumberger, D. Dolinar, A. Hamler, and M. Trlep: “Evaluation of Saturation and Cross-Magnetization Effects in Interior Permanent-Magnet Synchronous Motor”, *IEEE Trans. Ind. Applicat.*, Vol.39, No.5, pp.1264–1271 (2003)

(5) O.M. Mohammed, S.L. Liu, and Z. Liu: “A Phase Variable Model of Brushless dc Motors Based on Finite Element Analysis and Its Coupling with External Circuits”, *IEEE Trans. Magn.*, Vol.41, No.5, pp.1576–1579 (2005)

(6) G. Qi, J.T. Chen, Z.Q. Zhu, D. Howe, L.B. Zhou, and C.L. Gu: “Influence of Skew and Cross-Coupling on Flux-Weakening Performance of Permanent-Magnet Brushless AC Machines”, *IEEE Trans. Magn.*, Vol.45, No.5, pp.2110–2117 (2009)

(7) K. Akatsu and R.D. Lorenz: “Comparing Coupled Analysis with Experimental Results for an Interior PM Machine”, *IEEE Trans. Ind. Applicat.*, Vol.45, No.1, pp.178–185 (2009)

(8) G. Stumberger, B. Stumberger, D. Dolinar, and A. Hamler: “Cross Magnetization Effect on Inductances of Linear Synchronous Reluctance Motor Under Load Conditions”, *IEEE Trans. Magn.*, Vol.37, No.5, pp.3658–3662 (2001)

(9) M. Nashiki, Y. Inoue, Y. Kawai, and S. Okuma: “Inductance Calculation and New Modeling of a Synchronous Reluctance Motor Using Flux Linkages”, *IEEJ Trans.*, Vol.127-D, No.2, pp.158–166 (2007) (in Japanese)

(10) Investigating R&D Committee on Practical Analysis Techniques of 3-D Electromagnetic Field for Rotating Machines: “Practical Analysis Techniques of 3-D Electromagnetic Field for Rotating Machines”, *IEEJ Tech. Rep.*, No.1296 (2013)

Hiroyuki Kaimori (Member) received the M.S. degree from Toyo University, Japan, in 2002. Since April 2002, he joins at Science Solutions International Laboratory, Inc., Japan. He works for electromagnetic simulation software as a developer. His research interests are electromagnetic analysis and coupling analysis with circuit simulation of electrical machines. Mr. Kaimori is a member of IEEE.

Kan Akatsu (Member) received B.S., M.S., and Ph.D. degrees in electrical engineering from Yokohama National University, Yokohama, Japan, in 1995, 1997, 2000 respectively. He joined Nissan Research Center, Yokosuka, Japan, in 2000, he contributed to the design and analysis of the new concept permanent magnet machines. In 2003, he joined the department of Electrical and Electric Engineering at Tokyo University of Agriculture and Technology, Tokyo, Japan, as an assistant professor. From 2005 to 2007, he is a JSPS Postdoctoral Fellowship for Research Abroad, visiting professor in WEMPEC (Wisconsin Electric Machines and Power Electronics Consortium), University of Wisconsin Madison. From 2009, he is an associate professor in Shibaura Institute of Technology, Tokyo, Japan. His research interests are motor control, motor design and inverter control. Dr. Akatsu is a member of the IEEE PELS, IAS, IE.